Measurement 170 (2021) 108725

Contents lists available at ScienceDirect

Measurement

journal homepage: www.elsevier.com/locate/measurement

Constraint optimization algorithm for spectral emissivity calculation in multispectral thermometry

Nian Wang [a,b], Hua Shen [a,b,*], Rihong Zhu [a,b]

[a] School of Electronic and Optical Engineering, Nanjing University of Science and Technology, Nanjing 210094, China
[b] MIIT Key Laboratory of Advanced Solid Laser, Nanjing University of Science and Technology, Nanjing 210094, China

ARTICLE INFO

Keywords:
Emissivity
Temperature
Multispectral thermometry
Constraint optimization
Genetic algorithm

ABSTRACT

In multispectral thermometry, spectral emissivity calculation is crucial for temperature measurement. Constraint optimization algorithms require a shrunken emissivity search range and an appropriate initial solution to ensure high accuracy of temperature calculation. We propose a novel method without these requirements. In our method, the trend of the emissivity-wavelength curve is utilized to establish constraints, and a genetic algorithm is utilized as the optimization tool. Experiments reveal that the proposed method significantly improves the accuracy of temperature calculation for multispectral thermometry within a relative error of 1%. Our method can be applied to some high-precision temperature measurements (that require relative error less than 1%), such as the measurement of subtle variations in temperature distribution for aerospace engine plumes, and the measurement of slight changes in temperature during laser processing.

1. Introduction

Multispectral thermometry has advantages in terms of noncontact measurement, high-speed response, and simple device composition [1–5]. This technique has been employed in many fields, such as the component design of high-performance vehicles, quality control of laser processing, and performance evaluation of rocket engines [6–11]. Based on Planck's law, a set of equations can be constructed according to multispectral thermometry using the measured spectral radiation intensities at several wavelengths. This set contains N equations but $N + 1$ unknowns: N spectral emissivities at different wavelengths, and the temperature of the target [12,13]. Consequently, the equations are underdetermined and difficult to solve.

Traditional approaches follow the principle that an additional hypothesized relationship between emissivity and wavelength or temperature, that is, an emissivity assumption model, should be applied to address this problem. The hypothesis model between emissivity and wavelength can be in the form of polynomials, logarithm polynomials, or Fourier series [14–17]. After these models are applied onto the underdetermined equations such that the equations become determined or overdetermined, a data processing method based on equation solving [18–25] or least-square fitting [26–32], may be used to calculate the temperature. Models between emissivity and temperature have also been proposed based on the assumption that emissivity has a linear relationship with the continuous temperature in two consecutive time periods [33–36]. A problem with using emissivity models is that the calculation accuracies for emissivity and temperature will deteriorate if the adopted assumption model is not suitable.

Constraint optimization algorithms, which do not rely on emissivity assumption models, have thus been recently developed. A gradient projection (GP) algorithm, an internal penalty function (IPF) algorithm, and a generalized inverse matrix–exterior penalty function (GIM-EPF) algorithm have been proposed to avoid fixing the emissivity model in advance in the temperature calculations [37,38]. Although emissivity assumption models are no longer required, constraint optimization algorithms require estimation of the emissivity search range and selection of an appropriate initial solution of emissivity to determine the temperature. When the search range for emissivity is shrunk in alignment with reality and the initial solution of emissivity is selected appropriately, the accuracy is high; otherwise, a significant reduction in accuracy is observed.

This study aims to develop an optimization algorithm that requires neither the shrinking of the emissivity search range nor the selection of an appropriate initial solution and that can also ensure high accuracies for the emissivity and temperature calculations. In our method, the tendency of change in emissivity is considered when constraints are built, and a genetic algorithm (GA) is adopted to solve the objective function. Calculations of emissivity and temperature are performed on

* Corresponding author at: School of Electronic and Optical Engineering, Nanjing University of Science and Technology, Nanjing 210094, China.
E-mail address: edward_bayun@163.com (H. Shen).

https://doi.org/10.1016/j.measurement.2020.108725
Received 7 July 2020; Received in revised form 13 October 2020; Accepted 11 November 2020
Available online 19 November 2020

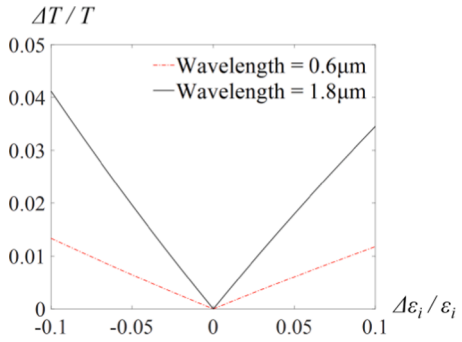

Fig. 1. . Relationship between relative uncertainty of spectral emissivity and corresponding relative uncertainty of temperature measurement for short (0.6 μm) and long (1.8 μm) wavelengths at 3000 K.

six hypothetical materials with different types of typical spectral emissivity distributions and one real material (tungsten) to verify the reliability of our method.

2. Method

2.1. Multispectral thermometry

According to Planck's law of blackbody radiation, the spectral radiation exitance$M(\lambda, T)$at wavelength λ and temperature T for a blackbody is expressed as follows:

$$M(\lambda,T)=\varepsilon\cdot C_1\lambda^{-5}\left(exp\frac{C_2}{\lambda T}-1\right)^{-1}, \tag{1}$$

where $C_1 = 3.742 \times 10^8$ W μm^4 m^{-2}, $C_2 = 14388$ μm K, and ε is the spectral emissivity of the target at temperature T and wavelength λ_i.

Based on Eq. (1), equations can be constructed using spectral radiation exitance M_i measured at several working wavelengths λ_i corresponding to different spectral channels and then transformed to Eq. (2) when the Wien approximation is satisfied.

$$M_i=\varepsilon_i\cdot C_1{\lambda_i}^{-5}exp\frac{-C_2}{\lambda_i T}, i=1,2\ldots n, \tag{2}$$

where ε_i is the emissivity of spectral channel i. There are n equations, but $n + 1$ unknowns in Eq. (2), indicating that the equation is an underdetermined equation and cannot be solved directly. Traditional methods assume certain functional relationships between emissivity ε and wavelength λ or temperature T. Thus, a model for the emissivity can be constructed and applied onto the set of equations to solve Eq. (2). However, if the model is not consistent with reality, the accuracy of the resulting temperature calculation will be significantly reduced [39,40]. The curve of the relationship between the relative uncertainty $\Delta\varepsilon_i/\varepsilon_i$ of spectral emissivity and the corresponding relative uncertainty $\Delta T/T$ of temperature measurement can be plotted according to Eq. (2), as shown in Fig. 1.

As shown in Fig. 1, if the temperature measurement is performed at long wavelengths, the relative error of the temperature measurement will exceed 4% when the relative error of spectral emissivity is greater than 10%, which is unacceptable. In most industrial applications, the required accuracy for temperature measurement is 1% or less. To overcome the disadvantages of using an emissivity model, constrained optimization algorithms have thus been recently developed. In this study, we propose a novel approach to constructing constraints using the varying trend of the emissivity.

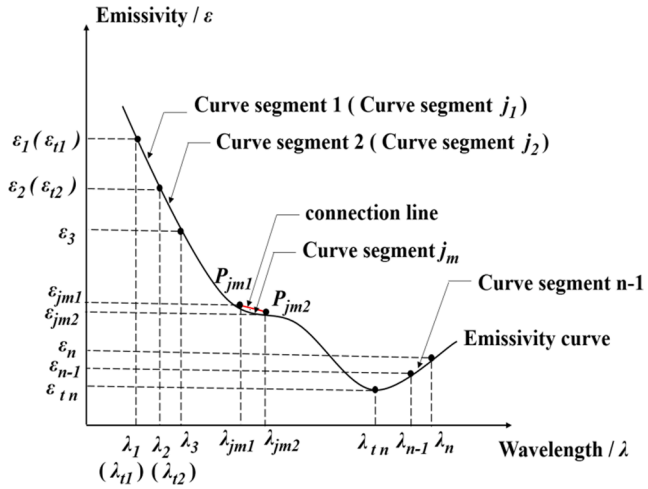

Fig. 2. Identification of parameters related to emissivity–wavelength curve.

2.2. Principle of proposed algorithm

2.2.1. Construction of objective function

Constraint optimization can be defined as follows:

$$minf(x)$$

$$s.\ t.\ Ax \geqslant b$$

where $f(x)$ is the objective function subject to the linear constraint condition $\boldsymbol{Ax} \geq \boldsymbol{b}$, $\boldsymbol{A}$ is the constraint coefficient matrix, $\boldsymbol{b}$ is the constraint vector, and $\boldsymbol{x}$ is the optimization variable. In particular, the constraint optimization problem aims to find an optimal vector $\boldsymbol{x}$ to minimize the objective function $f(x)$ under the constraint condition $\boldsymbol{Ax} - \boldsymbol{b} \geq \boldsymbol{0}$.

After logarithmic operations are performed on both sides of Eq. (2), the temperature T_i derived by each spectral channel is

$$T_i=\frac{C_2}{\lambda_i}\left(ln\varepsilon_i+ln\frac{C_1}{\lambda_i^5}-lnM_i\right)^{-1} \tag{3}$$

The objective function f is then constructed as follows:

$$f=\frac{1}{n}\sum_{i=1}^{n}\left(T_i-\overline{T}_E\right)^2 \tag{4}$$

where T_E is the average value of the temperature T_i calculated for each channel. When ε_i equals the real value, T_i will be equal to the true temperature, and the minimum value of f, expressed by min$f$, is obtained. The problem of solving Eq. (2) can therefore be converted into an optimization problem, with Eq. (4) as its objective function, and $\boldsymbol{\varepsilon}$ ($\boldsymbol{\varepsilon} = [\varepsilon_1\ \varepsilon_2 \cdots \varepsilon_n]^T$) as its optimization variable, following certain constraints.

2.2.2. Construction of constraints

Our constraints are derived based on the following two aspects.

First, the emissivity should obey $0 < \varepsilon_i < 1$; thus, the constraints are expressed as follows:

$$\begin{aligned}\varepsilon_i &> 0\\ -\varepsilon_i &> -1\end{aligned} \tag{5}$$

Second, according to the measurement data on the emissivities of various materials at different temperatures and wavelengths [41–45], we assume that although emissivity varies with temperature and surface state, the trend of its variation with wavelength is similar for a particular material at different temperatures. Based on known emissivity values for different wavelengths at certain temperatures reported in literature, the characteristics of the emissivity–wavelength curve trend can be extrapolated to

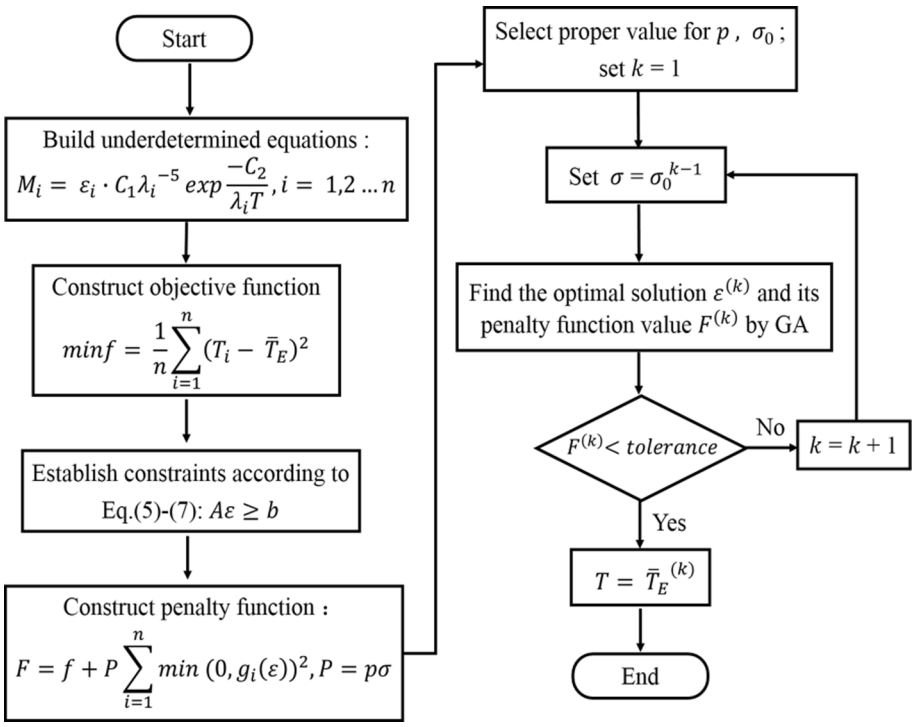

Fig. 3. Flow chart for the proposed algorithm.

establish the following constraints for the calculation of other unknown temperatures and corresponding emissivities:

a. The descending order of the spectral emissivities of the channels is

$$\varepsilon_{t_1} > \varepsilon_{t_2} > \cdots > \varepsilon_{t_n},\ t_1 \neq t_2 \neq \cdots \neq t_n,\ t_1,\ t_2 \cdots t_n \in \{1, 2 \cdots n\}, \tag{6}$$

where n denotes the total number of spectral channels, $t_1, t_2 \cdots t_n$ denote the serial numbers of the different spectral channels, and $\varepsilon_{t1}, \varepsilon_{t2} \cdots \varepsilon_{tn}$ denote the spectral emissivities of the different channels corresponding to wavelengths $\lambda_{t1}, \lambda_{t2} \cdots \lambda_{tn}$, respectively. These parameters are detailed in Fig. 2.

b. The descending order of the degrees of steepness of the curve segments between two neighboring working wavelengths is

$$|k_{j_1}| > |k_{j_2}| > \cdots > |k_{j_m}|, j_1 \neq j_2 \neq \cdots \neq j_m, j_1,\ j_2 \cdots j_m \in \{1, 2 \cdots (n\text{-}1)\},$$

$$k_{j_1} = \frac{\varepsilon_{j_{12}} - \varepsilon_{j_{11}}}{\lambda_{j_{12}} - \lambda_{j_{11}}},\ k_{j_2} = \frac{\varepsilon_{j_{22}} - \varepsilon_{j_{21}}}{\lambda_{j_{22}} - \lambda_{j_{21}}},\ k_{j_m} = \frac{\varepsilon_{j_{m2}} - \varepsilon_{j_{m1}}}{\lambda_{j_{m2}} - \lambda_{j_{m1}}},\ m = n - 1, \tag{7}$$

where $j_1, j_2 \cdots j_m$ denote the serial numbers of the different curve segments; $j_{11}, j_{21} \cdots j_{m1}$ denote the serial numbers of the left end points of the different curve segments; $j_{12}, j_{22} \cdots j_{m2}$ denote the serial numbers of the right end points of the different curve segments; and $k_{j1}, k_{j2} \cdots k_{jm}$ denote the slopes of the connection lines between the end points of the curve segments, with their absolute values representing the degrees of steepness of the curve segments. These parameters are shown in Fig. 2. λ_{jm1} and ε_{jm1} represent the wavelength and emissivity, respectively, of the left end point P_{jm1} of the curve segment j_m, whereas λ_{jm2} and ε_{jm2} represent those of the right end point P_{jm2}.

After the inequality constraints in Eqs. (5)–(7) for the optimization variable $\boldsymbol{\varepsilon}$ are addressed, the constraint coefficient matrix $\boldsymbol{A}$ and constraint matrix $\boldsymbol{b}$ may be obtained. In combination with the objective function determined using Eq. (4), the constrained optimization problem of solving the temperature and emissivity based on multispectral thermometry is then summarized as follows:

$$minf = \frac{1}{n}\sum_{i=1}^{n}\left(T_i - \overline{T}_E\right)^2$$

$$s.\ t.\ Ax \geqslant b. \tag{8}$$

2.2.3. Solution for constrained optimization problem

The exterior penalty function method is a common method for solving constraint optimization problems. In this method, the original objective function is combined with a penalty term that is constructed depending on the constraints, forming the penalty function into a new optimization objective function. Here, the penalty function F is defined as follows:

$$F = f + P\sum_{i=1}^{N}\left(min(0, g_i(\varepsilon))\right)^2,$$

$$g_i(\varepsilon) = A_i\varepsilon - b_i,$$

$$P = p\sigma, p > 0, \sigma > 0, \tag{9}$$

where f is the original objective function determined using Eq. (8), $P\sum_{i=1}^{N}\left(min(0, g_i(\varepsilon))\right)^2$ is the penalty term, A_i is the component of row i of the constraint coefficient matrix $\boldsymbol{A}$, b_i is the i-th component of the constraint vector b, and ε is the optimization variable. Moreover, $\boldsymbol{A}$, $\boldsymbol{b}$, and ε are all determined using Eq. (8); N is the number of rows of matrix $\boldsymbol{A}$ or, in other words, the number of constraint conditions; and P is the penalty factor given by the product of two positive parameters p and σ, where p is constant and σ increases gradually as the iteration continues.

In the calculation process, the penalty term will be positive, leading to an increase in the value of the new objective function when the solution does not meet the constraints (implying that it is an infeasible solution), in which case the punishment is implemented. As the iteration continues, the punishment becomes increasingly severe along with an increase in the penalty factor P, forcing the search direction to turn away from infeasible solutions toward feasible solutions. Finally, an optimal solution that meets the constraints is determined.

Essentially, the constrained optimization problem presented by Eq. (8) is transformed into the nonconstrained optimization problem in Eq. (9), based on the exterior penalty function method. In the search for an optimal solution for the new objective function (the penalty function F in

Table 1
Emissivity values of different types of hypothetical materials at 1800 K.

Material	λ_1 0.4 μm	λ_2 0.5 μm	λ_3 0.6 μm	λ_4 0.7 μm	λ_5 0.8 μm	λ_6 0.9 μm	λ_7 1.0 μm	λ_8 1.1 μm
A	0.85	0.75	0.67	0.6	0.55	0.5	0.48	0.45
B	0.45	0.48	0.5	0.55	0.6	0.67	0.75	0.85
C	0.45	0.55	0.65	0.75	0.74	0.65	0.55	0.45
D	0.85	0.75	0.65	0.55	0.54	0.65	0.75	0.8
E	0.85	0.65	0.55	0.65	0.84	0.65	0.55	0.5
F	0.5	0.55	0.65	0.84	0.65	0.55	0.65	0.85

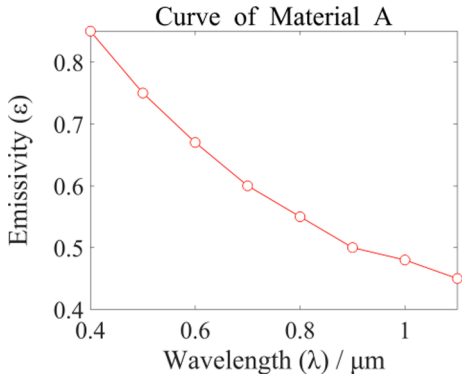

Fig. 4. Emissivity–wavelength curve for hypothetical material A at 1800 K.

Eq. (9)), previous optimization algorithms for multispectral thermometry are characterized by local optimization, which requires the selection of the initial solution to be optimized for the iteration. However, the precision is significantly reduced if the selected initial solution is not suitable.

To address this problem, the proposed method utilizes a GA that performs global searches in solving for the objective function F. The GA begins its iteration with randomly generated solutions, thus omitting the selection of an initial solution, which makes the proposed method more convenient than standard approaches. The GA adopted in the proposed method is presented in detail in Ref. [46].

The proposed algorithm is visualized using the flow chart in Fig. 3.

3. Results

3.1. Calculations for materials with different emissivity models

To verify the flexibility of our method to be used with various materials, temperature calculations were conducted for six hypothetical materials with different emissivity–wavelength trends. The emissivity values assigned to these materials at a temperature of 1800 K are shown in Table 1, presenting various typical distribution modes, such as increasing, decreasing, convex wave, concave wave, M wave, and W wave. From the emissivity values in Table 1, the values of spectral radiation exitances at wavelengths λ_1–λ_8 can be derived to simulate measured data for these materials. With the values of spectral radiation exitances, the temperature and emissivity of the six materials can be calculated using our method and compared with the values in Table 1.

If material A is used as an example, the calculation process proceeds as follows.

Based on the spectral emissivity ε_A of material A at each wavelength in Table 1, the emissivity–wavelength curve is presented, as shown in Fig. 4. The descending order of spectral emissivity values is expressed as follows:

$$\varepsilon_{A_1} > \varepsilon_{A_2} > \varepsilon_{A_3} > \varepsilon_{A_4} > \varepsilon_{A_5} > \varepsilon_{A_6} > \varepsilon_{A_7} > \varepsilon_{A_8} \tag{10}$$

The above equation can be expressed in matrix form.

$$M_{A1}\varepsilon_A > b_{A1}$$

$$M_{A1} = \begin{bmatrix} M_{A11} \\ M_{A12} \\ \vdots \\ M_{A17} \end{bmatrix}, M_{A11} = \begin{bmatrix} 1\ -1\ 0\ \cdots\ 0 \\ 1\ 0\ -1\ \cdots\ 0 \\ \cdots \\ 1\ 0\ \cdots\ -1 \end{bmatrix}_{7\times 8}, M_{A12} = \begin{bmatrix} 0\ 1\ -1\ 0\ \cdots\ 0 \\ 0\ 1\ 0\ -1\ \cdots\ 0 \\ \cdots \\ 0\ 1\ 0\ \cdots\ -1 \end{bmatrix}_{6\times 8}$$

$$M_{A17} = [0\ \cdots\ 0\ 1\ \ -1\ ]_{1\times 8},\ \varepsilon_A = \left[\varepsilon_{A_1}\ \varepsilon_{A_2}\cdots\varepsilon_{A_8}\right]^T, b_{A1} = 0_{28\times 1} \tag{11}$$

In addition, the absolute values of the slopes of the lines connecting the two ends of each of the curve segments are sorted as follows:

$$\left|k_{A_{j_1}}\right| > \left|k_{A_{j_2}}\right| > \left|k_{A_{j_3}}\right| > \left|k_{A_{j_4}}\right| = \left|k_{A_{j_5}}\right| > \left|k_{A_{j_6}}\right| > \left|k_{A_{j_7}}\right|$$

$$\begin{aligned} k_{A_{j_1}} &= \frac{\varepsilon_{A_2}-\varepsilon_{A_1}}{\lambda_2-\lambda_1}, k_{A_{j_2}} = \frac{\varepsilon_{A_3}-\varepsilon_{A_2}}{\lambda_3-\lambda_2}, k_{A_{j_3}} = \frac{\varepsilon_{A_4}-\varepsilon_{A_3}}{\lambda_4-\lambda_3}, k_{A_{j_4}} = \frac{\varepsilon_{A_5}-\varepsilon_{A_4}}{\lambda_5-\lambda_4}, \\ k_{A_{j_5}} &= \frac{\varepsilon_{A_6}-\varepsilon_{A_5}}{\lambda_6-\lambda_5}, k_{A_{j_6}} = \frac{\varepsilon_{A_8}-\varepsilon_{A_7}}{\lambda_8-\lambda_7}, k_{A_{j_7}} = \frac{\varepsilon_{A_7}-\varepsilon_{A_6}}{\lambda_7-\lambda_6}. \end{aligned} \tag{12}$$

The second constraint in Eq. (12) can be constructed as follows:

$$\left|\frac{\varepsilon_{A_2}-\varepsilon_{A_1}}{\lambda_2-\lambda_1}\right| > \left|\frac{\varepsilon_{A_3}-\varepsilon_{A_2}}{\lambda_3-\lambda_2}\right|,\ \left|\frac{\varepsilon_{A_3}-\varepsilon_{A_2}}{\lambda_3-\lambda_2}\right| \rangle \left|\frac{\varepsilon_{A_4}-\varepsilon_{A_3}}{\lambda_4-\lambda_3}\right|,\ \left|\frac{\varepsilon_{A_4}-\varepsilon_{A_3}}{\lambda_4-\lambda_3}\right| \rangle \left|\frac{\varepsilon_{A_5}-\varepsilon_{A_4}}{\lambda_5-\lambda_4}\right|,$$

$$\left|\frac{\varepsilon_{A_6}-\varepsilon_{A_5}}{\lambda_6-\lambda_5}\right| > \left|\frac{\varepsilon_{A_8}-\varepsilon_{A_7}}{\lambda_8-\lambda_7}\right|,\ \left|\frac{\varepsilon_{A_8}-\varepsilon_{A_7}}{\lambda_8-\lambda_7}\right| \rangle \left|\frac{\varepsilon_{A_7}-\varepsilon_{A_6}}{\lambda_7-\lambda_6}\right| \tag{13}$$

Transferring Eq. (13) to the matrix form, we obtain

$$M_{A2}\varepsilon_A > b_{A2},$$

$$M_{A2} = \begin{bmatrix} 1\ -2\ 1\ 0\ 0\ 0\ 0\ 0 \\ 0\ 1\ -2\ 1\ 0\ 0\ 0\ 0 \\ 0\ 0\ 1\ -2\ 1\ 0\ 0\ 0 \\ 0\ 0\ 0\ 0\ 1\ -1\ -1\ 1 \\ 0\ 0\ 0\ 0\ 0\ -1\ 2\ -1 \end{bmatrix}, b_{A2} = 0_{5\times 1} \tag{14}$$

The last and natural constraint is $0 < \varepsilon_{Ai} < 1$ ($i = 1, 2 \cdots 8$), which can be written in the matrix form as follows:

$$M_{A3}\varepsilon_A > b_{A3},$$

$$M_{A3} = \begin{bmatrix} 1\ 0\ 0\ 0\ 0\ 0\ 0\ 0 \\ -1\ 0\ 0\ 0\ 0\ 0\ 0\ 0 \\ 0\ 1\ 0\ 0\ 0\ 0\ 0\ 0 \\ 0\ -1\ 0\ 0\ 0\ 0\ 0\ 0 \\ \cdots \\ 0\ 0\ 0\ 0\ 0\ 0\ 0\ 1 \\ 0\ 0\ 0\ 0\ 0\ 0\ 0\ -1 \end{bmatrix}_{16\times 8},$$

$$b_{A3} = [0\ -1\ 0\ -1\ 0\ -1\ 0\ -1\ 0\ -1\ 0\ -1\ 0\ -1\ 0\ -1]^T. \tag{15}$$

The entire set of constraint conditions can then be summarized as follows:

$$A_A\varepsilon_A > b_A\ ,$$

$$A_A = \begin{bmatrix} M_{A1} \\ M_{A2} \\ M_{A3} \end{bmatrix}, b_A = \begin{bmatrix} b_{A1} \\ b_{A2} \\ b_{A3} \end{bmatrix}, \varepsilon_A = \left[\varepsilon_{A_1}\ \varepsilon_{A_2}\cdots\varepsilon_{A_8}\right]^T \tag{16}$$

After the constraint conditions are established, the penalty function of material A can be constructed as follows:

$$F_A = f_A + P_A \sum_{i=1}^{49} \left(min(0, g_{Ai}(\varepsilon_A))\right)^2, \tag{17}$$

where f_A is the original objective function determined using Eq. (8), $g_{Ai}(\varepsilon_A) = A_{Ai}\varepsilon_A - b_{Ai}$, $A_{Ai}$is the component of row i of the constraint coefficient matrix A_A, and b_{Ai} is the i-th component of the constraint

Table 2
Temperature calculation results for different kinds of hypothetical materials.

Material	A	B	C	D	E	F
Temperature calculated (K)	1794.9	1803.1	1791.4	1810.3	1805.7	1805.0
Relative error (%)	0.29	0.17	0.48	0.57	0.32	0.28

vector b_A.

The subsequent steps of the algorithm (shown in Fig. 3) are then executed for material A, wherein the corresponding parameters of the iterative process are set to $p = 0.05$ and $\sigma_0 = 3$, and the iteration termination condition was $Tolerance = 10^{-6}$. The simulation results are listed in Table 2. The calculation results for materials B–F, for which similar calculation processes are used, are also presented in Table 2.

The spectral emissivity calculation results for six hypothetical materials are shown in Fig. 5, with the corresponding root-mean-square (RMS) relative errors listed in Table 3. The RMS relative error is defined as follows:

$$E_{RMS} = \sqrt{\frac{\sum_{i=1}^{8} [(\varepsilon_{ri} - \varepsilon_i)/\varepsilon_{ri}]^2}{8}}, \tag{18}$$

where ε_{ri} denotes the actual value of each spectral channel and $\varepsilon_i$represents the resolved value.

As shown in Table 2, the relative errors of the temperature calculation are less than 1% for all materials, whereas the RMS relative errors for the emissivities are less than 7%, as presented in Table 3. In addition, the emissivity–wavelength curves of the different hypothetical materials

Table 3
RMS relative errors for calculated emissivities.

Material	A	B	C	D	E	F
E_{RMS} (%)	3.67	2.16	6.25	6.86	3.9	3.4

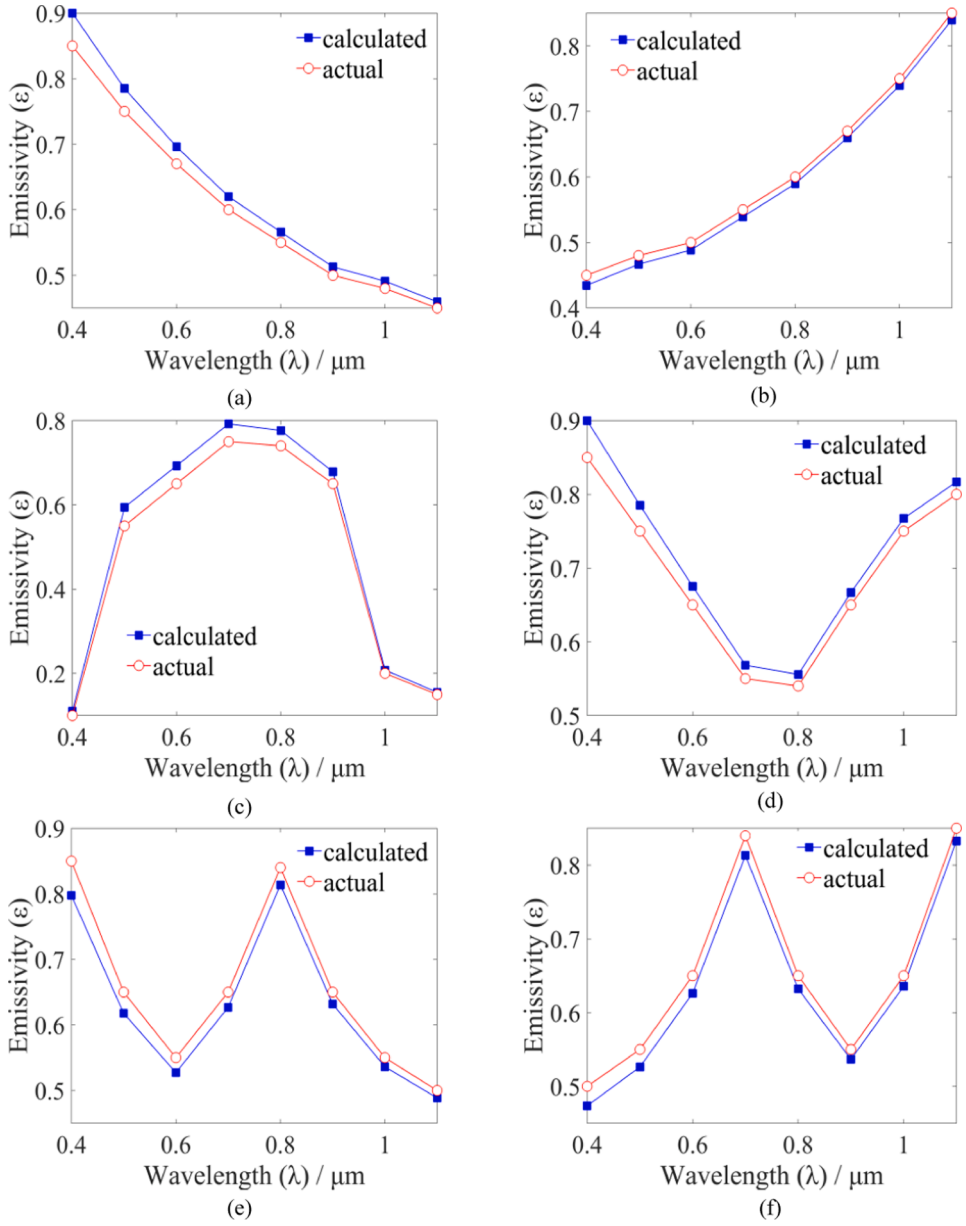

Fig. 5. Calculation results. Comparison between calculated and actual values of spectral emissivity for (a) material A, (b) material B, (c) material C, (d) material D, (e) material E, and (f) material F.

Table 4
Spectral emissivity data for tungsten (from [47]).

Temperature (K)	λ_1	λ_2	λ_3	λ_4	λ_5	λ_6	λ_7	λ_8
	0.3 μm	0.38 μm	0.467 μm	0.665 μm	0.8 μm	1.0 μm	1.5 μm	1.8 μm
1200	0.503	0.495	0.482	0.452	0.428	0.39	0.275	0.177
1800	0.500	0.488	0.472	0.439	0.417	0.382	0.284	0.206
2500	0.493	0.477	0.462	0.425	0.405	0.375	0.295	0.240
2800	0.490	0.473	0.458	0.419	0.399	0.371	0.299	0.254
3000	0.488	0.47	0.455	0.415	0.396	0.368	0.302	0.264

Table 5
Temperature and emissivity results for tungsten calculated using the proposed method.

Actual temperature (K)	1800	2500	2800	3000
T_c (K)	1806.0	2486.6	2817.1	2970.5
ΔT_R (%)	0.33	0.54	0.61	0.98
$\Delta\varepsilon_{RMS}$ (%)	4.8	6.05	5.64	9.50

T_c: calculated temperature, ΔT_R: relative error for calculated temperature results, $\Delta\varepsilon_{RMS}$: RMS relative errors for calculated emissivity results.

calculated using our algorithm are close to the actual distribution curve shown in Fig. 5. When these results are considered, the feasibility and validity of our method are verified by these simulations.

3.2. Calculations for tungsten

To verify whether our algorithm can effectively obtain the temperature of a real target in a practical application, a temperature calculation was conducted using tungsten because it is a widely used material. The known spectral emissivity values of tungsten at certain temperatures are referenced from literature [47] and are listed in Table 4. The varying trend of the emissivity at a temperature of 1200 K was employed to construct the constraint conditions. The corresponding temperature and emissivity values of tungsten were then calculated using the proposed method, with the derived spectral radiation exitances for different wavelengths at 1800, 2500, 2800, and 3000 K to compare with the actual values.

The temperature results calculated using the proposed method and the RMS relative errors for the calculated emissivity results are listed in Table 5. A comparison of the calculated and actual emissivity–wavelength curves is shown in Fig. 6.

As shown in Table 5, the relative errors for the calculated temperatures obtained using the proposed method are less than 1%, whereas the RMS relative errors for the calculated emissivity values obtained using the proposed method are less than 10%. In addition, Fig. 6 reveals that the emissivity–wavelength curves obtained via our algorithm at different temperatures are consistent with the trends of the actual value curves. These findings indicate the accuracy and efficacy of the proposed method in practical applications. However, errors for spectral emissivity are noticeably higher at shorter wavelengths. The reason can be determined from the objective function f, represented by Eq. (4), and the relationship between $\Delta\varepsilon_i/\varepsilon_i$ and $\Delta T/T$, as shown in Fig. 1. According to the objective function f, the algorithm optimization aims to ensure that the calculated temperature for each channel tends toward the same value (i.e., true value). Meanwhile, as shown in Fig. 1, the longer the wavelength, the greater the calculated relative temperature error $\Delta T/T$

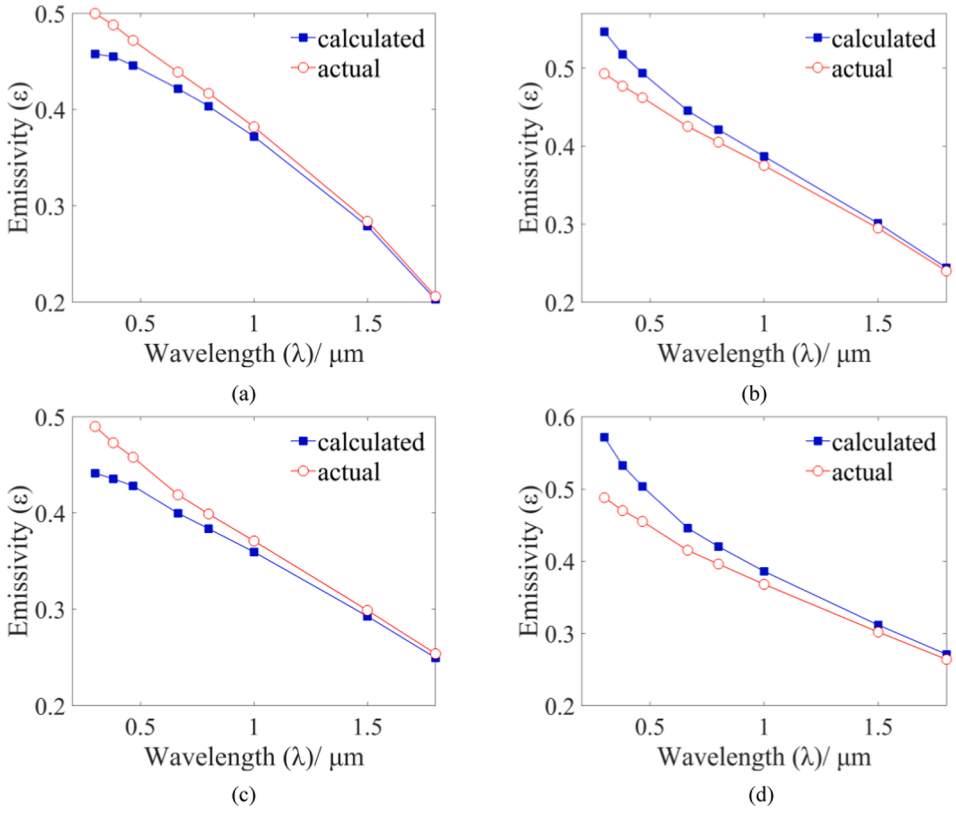

Fig. 6. Comparison of emissivity–wavelength curves calculated using the proposed method and actual values at (a) 1800 K, (b) 2500 K, (c) 2800 K, and (d) 3000 K.

caused by the relative error $\Delta\varepsilon_i / \varepsilon_i$ for the corresponding spectral emissivity. When the spectral emissivity at a long wavelength has a slight error, the temperature will change significantly. However, even if there is a large deviation in the emissivity at a short wavelength, the temperature will not change exceedingly. As the calculated temperature gradually converges to the true value, the improvement of emissivities at long wavelengths is better than that at short wavelengths, resulting in errors for the emissivities at short wavelengths becoming greater by the time the iteration stops.

4. Conclusions

In this study, a novel constraint optimization algorithm, the constraints of which are constructed using the varying trend of the emissivity, is proposed. The advantages of our method are as follows. 1. The specific range of emissivity need not be determined before temperature calculation. 2. The optimization of an initial solution is not required; therefore, our method has better environmental applicability. 3. The temperature calculation accuracy is within 1% relative error. The experimental results demonstrate that the accuracy of multispectral thermometry is remarkably improved by our method. Because of these advantages, our method can be applied to some high-precision temperature measurements that require a relative error less than 1%. For example, the proposed method can be used to distinguish subtle variations in the temperature distribution of aerospace engine plume, helping to understand the reaction inside the plume to improve the formulation of the propellant. The method can also be used to measure slight temperature changes during laser processing, assisting operators in adjusting the processing parameters in a timely manner to achieve better welding quality.

CRediT authorship contribution statement

Nian Wang: Writing - review & editing, Data curation. **Hua Shen:** Methodology. **Rihong Zhu:** Resources.

Declaration of Competing Interest

The authors declare that they have no known competing financial interests or personal relationships that could have appeared to influence the work reported in this paper.

Acknowledgment

This study was funded by the National Key Research and Development Program of China (2017YFB1104400).

References

[1] J.L. Urban, M. Vicariotto, D. Dunn-Rankin, A.C. Fernandez-Pello, Temperature measurement of glowing embers with color pyrometry, Fire. Technol. 55 (2019) 1013–1026.
[2] A. Akbarnozari, F. Ben-Ettouil, S. Amiri, O. Bamber, J.-D. Grenon, M. Choquet, L. Pouliot, C. Moreau, Online diagnostic system to monitor temperature of in-flight particles in suspension plasma spray, J. Therm. Spray Technol. 29 (2020) 908–920.
[3] M. Szulc, S. Kirner, G. Forster, J. Schein, A novel approach to determine in-flight particle oxidation for thermal spraying processes, J. Therm. Spray Technol. 29 (2020) 932–946.
[4] B. Bouvry, G. Cheymol, L. Ramiandrisoa, C. Gallou, H. Maskrot, N. Horny, T. Duvaut, C. Destouches, L. Ferry, C. Gonnier, Multispectral pyrometry for surface temperature measurement of oxidized Zircaloy claddings, Infrared Phys. Technol. 83 (2017) 78–87.
[5] T.R. Fu, J.F. Liu, A.Z. Zong, Radiation temperature measurement method for semitransparent materials using one-channel infrared pyrometer, Appl. Opt. 53 (2014) 6830–6839.
[6] T.R. Fu, J.F. Liu, M.H. Duan, S. Li, Sub-pixel temperature measurements in hypersonic plasma jet environments using high speed multispectral pyrometry, J. Heat Transfer 140 (2018) 1601–1609.
[7] D.J. Dagel, G.D. Grossetete, D.O. MacCallum, S.P. Korey, Four-color imaging pyrometer for mapping temperatures of laser-based metal processes, Pros. SPIE 9861 (2016), 986103.
[8] N. Wang, H. Shen, R.H. Zhu, Spectral radiation transmission model of plasma in laser welding, Spectrosc. Spect. Anal. 40 (2020) 1362–1366.
[9] M. Liang, B.J. Sun, X.G. Sun, J.Y. Xie, Development of a new fiber-optic multi-target multispectral pyrometer for achievable true temperature measurement of the solid rocket plume, Measurement 95 (2017) 239–245.
[10] Y.W. Huang, M.J. Long, H.L. Fan, L.T. Gui, D.F. Chen, H.M. Duan, Quantifying the effects of combustion gases' radiation on surface temperature measurements using two-color pyrometry, Energy Fuels 33 (2019) 3610–3619.
[11] M.V. Mekhrengin, I.K. Meshkovskii, V.A. Tashkinov, V.I. Guryev, A.V. Sukhinets, D.S. Smirnov, Multispectral pyrometer for high temperature measurements inside combustion chamber of gas turbine engines, Measurement 139 (2019) 355–360.
[12] P.B. Coates, The least-square approach to multi-wavelength pyrometry, High Temp. High Press. 20 (1988) 433–441.
[13] A. Araújo, Analysis of multiband pyrometry for emissivity and temperature measurements of gray surfaces at ambient temperature, Infrared Phys. Technol. 76 (2016) 365–374.
[14] D.Y. Svet, Determination of the emissivity of a substance from the spectrum of its thermal radiation and optimal methods of optical pyrometry, High Temp. High Press. 8 (1976) 493–498.
[15] C.D. Wen, Y.H. Chr, The assessment of multispectral radiation thermometry using linear and loglinear emissivity models for steel, Numer. Heat Transfer B 58 (2010) 40–54.
[16] C.D. Wen, T.Y. Chai, Experimental investigation of emissivity of aluminum alloys and application of multispectral radiation thermometry, Appl. Therm. Eng. 31 (2011) 2414–2421.
[17] P.B. Coates, Multi-wavelength pyrometry, Metrologia 17 (1981) 103–109.
[18] M.A. Khan, C. Allemand, T.W. Eagar, Noncontact temperature measurement. I. Interpolation based techniques, Rev. Sci. Instrum. 62 (1991) 392–402.
[19] H. Madura, M. Kastek, T. Piatkowski, Automatic compensation of emissivity in three-wavelength pyrometers, Infrared Phys. Technol. 51 (2007) 1–8.
[20] A. Tapetado, J. Diaz-Alvarez, M.H. Miguelez, C. Vazquez, Two-color pyrometer for process temperature measurement during machining, J. Lightwave Technol. 34 (2016) 1380–1386.
[21] D. Ketui, F. Chi, G. Shan, Single wavelength and ratio pyrometry reflection errors in temperature measurement of gas turbine blade, Measurement 86 (2016) 133–140.
[22] Z.Z. Zhu, H. Shen, N. Wang, Transient measure technique for excitation temperature and radiation temperature based on multi-spectral method, Spectrosc. Spect. Anal. 2 (2018) 333–339.
[23] Z.Z. Zhu, H. Shen, N. Wang, Radiation temperature measurement technology based on the basis of spectral emissivity function, Spectrosc. Spect. Anal. 37 (2017) 685–691.
[24] A. Araújo, R. Silva, Surface temperature estimation in determined multi-wavelength pyrometry systems, Rev. Sci. Instrum. 91 (2020), 054901.
[25] Y. Zhai, H. Shen, R.H. Zhu, Development of transient pyrometer based on multi-spectral radiation technology, Spectrosc. Spect. Anal. 11 (2010) 3161–3165.
[26] J.L. Gardner, Computer modelling of a multi-wavelength pyrometer for measuring true surface temperature, High Temp. High Press. 12 (1980) 669–705.
[27] M.A. Khan, C. Allemand, T.W. Eagar, Noncontact temperature measurement. II. Least squares based techniques, Rev. Sci. Instrum. 62 (1991) 403–409.
[28] D.Y. Svet, S.S. Sergeev, A triple-wavelength pyrometer that measures true temperature, Meas. Tech. 54 (2012) 1273–1275.
[29] W. Devesse, D.D. Baere, P. Guillaume, High resolution temperature measurement of liquid stainless steel using hyperspectral imaging, Sensors 17 (2017) 91.
[30] K. Daniel, C. Feng, S. Gao, Application of multispectral radiation thermometry in temperature measurement of thermal barrier coated surfaces, Measurement 92 (2016) 218–223.
[31] W.J. Yan, K.Y. Li, X.L. Huang, L.B. Yu, C. Lou, Y.M. Chen, Online measurement of the flame temperature and emissivity during biomass volatile combustion using spectral thermometry and image thermometry, Energy Fuels 34 (2020) 907–919.
[32] Y.Z. Zhang, W.Q. Zhang, Z. Dong, S.B. Shu, X.L. Lang, L. Yang, Measurement performance analysis for a charge-coupled-device-based nearinfrared multi-spectral pyrometer, Infrared Phys. Technol. 106 (2020), 103273.
[33] X.G. Sun, G.B. Yuan, J.M. Dai, Z.X. Chu, Processing method of multi-wavelength pyrometer data for continuous temperature measurements, Int. J. Thermophys. 26 (2005) 1255–1261.
[34] J. Xing, S.L. Cui, W.G. Qi, F. Zhang, X.G. Sun, W.M. Sun, A data processing algorithm for multi-wavelength pyrometry-which does not need to assume the emissivity model in advance, Measurement 67 (2015) 92–98.
[35] J. Xing, R.S. Rana, W.H. Gu, Emissivity range constraints algorithm for multi-wavelength pyrometer (MWP), Opt. Express 24 (2016) 19185–19194.
[36] M. Liang, B. Sun, X. Sun, J. Xie, C. Yu, Rules of emissivity sample choice in multiwavelength pyrometry, Int. J. Thermophys. 38 (2017) 35.
[37] J. Xing, B. Peng, Z. Ma, X. Guo, L. Dai, W.H. Gu, W.L. Song, Directly data processing algorithm for multiwavelength pyrometer (MWP), Opt. Express 25 (2017) 30560–30574.
[38] J.F. Liang, L. Dai, S. Chen, W.H. Gu, B. Peng, N.N. Jiang, W.L. Song, J. Xing, Generalized inverse matrix-exterior penalty function (GIM-EPF) algorithm for data processing of multiwavelength pyrometer (MWP), Opt. Express 26 (2018) 25706–25720.
[39] C.D. Wen, I. Mudawar, Emissivity characteristics of roughened aluminum alloy surfaces and assessment of multispectral radiation thermometry (MRT) emissivity models, Int. J. Heat MassTrans. 47 (2004) 3591–3605.
[40] Th. Duvaut, Comparison between multiwavelength infrared and visible pyrometry: application to metals, Infrared Phys. Technol. 51 (2008) 292–299.

[41] G. Teodorescu, P.D. Jones, R.A. Overfelt, B.J. Guo, Normal emissivity of high-purity nickel at temperatures between 1440 and 1605 K, J. Phys. Chem. Solids 69 (2008) 133–138.
[42] O. Rozenbaum, D. De Sousa Meneses, Y. Auger, S. Chermanne, P. Echegut, A spectroscopic method to measure the spectral emissivity of semi-transparent materials up to high temperature, Rev. Sci. Instrum. 70 (1999) 4020–4025.
[43] L.D. Campo, R.B. Pérez-Sáez, M.J. Tello, X. Esquisabel, I. Fernández, Armco iron normal spectral emissivity measurements, Int. J. Thermophys. 27 (2006) 1160–1172.
[44] L. González-Fernández, E. Risueño, R.B. Perez-Saez, M.J. Tello, Infrared normal spectral emissivity of Ti–6Al–4V alloy in the 500–1150 K temperature range, J. Alloy. Compd 541 (2012) 144–149.
[45] F. Zhang, K. Yu, K.H. Zhang, Y.L. Liu, Y. Zhao, Y.F. Liu, Infrared spectral emissivity property of pure titanium in the 473–1035 K temperature range, Appl. Spectrosc. 70 (2016) 1717–1725.
[46] C.R. Houck, J.A. Joines, M.G. Kay, a genetic algorithm for function optimization: a Matlab implementation, NCSU-IE TR 95 (1995) 1–14.
[47] W.E. Forsythe, E.Q. Adams, Radiating characteristics of tungsten and tungsten lamps, J. Opt. Soc. Am. 35 (1945) 108–113.